GRAIN BOUNDARY CHEMISTRY AND INTERGRANULAR CORROSION IN ALLOY 825

Y.-M Pan, D.S. Dunn, G.A. Cragnolino, and N. Sridhar
Center for Nuclear Waste Regulatory Analyses
Southwest Research Institute
San Antonio, TX

ABSTRACT

Alloy 825, a candidate material for radioactive high-level waste containers, was investigated to assess its thermal stability and the time-temperature conditions for sensitization. Alloy specimens with a carbon content of 0.01 wt. % in the mill-annealed and solution-annealed conditions were studied after thermal exposure to temperatures in the range of 600 to 800°C for periods of up to 1,000 hours. Sensitization was evaluated by using corrosion tests that were correlated with grain boundary chemistry analyses. Sensitized microstructures were found to contain $M_{23}C_6$-type carbides and a chromium-depleted region in the vicinity of the grain boundaries. Thermal aging at 700°C for 100 hours resulted in the highest sensitization. Whereas low-temperature aging at 640°C showed a progressive development of sensitization with time, healing was found to occur after aging at 800°C for 100 hours. The degree of sensitization quantified by an equivalent chromium depletion zone size correlates well to both the corrosion rate in the nitric acid test and the repassivation potential in a chloride-containing solution. Thermodynamic models were used to calculate the interfacial

GRAIN BOUNDARY CHEMISTRY AND INTERGRANULAR CORROSION IN ALLOY 825

Y.-M Pan, D.S. Dunn, G.A. Cragnolino, and N. Sridhar
Center for Nuclear Waste Regulatory Analyses
Southwest Research Institute
San Antonio, TX

ABSTRACT

Alloy 825, a candidate material for radioactive high-level waste containers, was investigated to assess its thermal stability and the time-temperature conditions for sensitization. Alloy specimens with a carbon content of 0.01 wt. % in the mill-annealed and solution-annealed conditions were studied after thermal exposure to temperatures in the range of 600 to 800°C for periods of up to 1,000 hours. Sensitization was evaluated by using corrosion tests that were correlated with grain boundary chemistry analyses. Sensitized microstructures were found to contain $M_{23}C_6$-type carbides and a chromium-depleted region in the vicinity of the grain boundaries. Thermal aging at 700°C for 100 hours resulted in the highest sensitization. Whereas low-temperature aging at 640°C showed a progressive development of sensitization with time, healing was found to occur after aging at 800°C for 100 hours. The degree of sensitization quantified by an equivalent chromium depletion zone size correlates well to both the corrosion rate in the nitric acid test and the repassivation potential in a chloride-containing solution. Thermodynamic models were used to calculate the interfacial

chromium concentration, chromium depletion profile, and the depletion zone width. Comparisons between experimental measurements and model calculations indicate that reliable prediction depends on the selection of key model parameters.

I. INTRODUCTION

The thermal stability of nuclear waste container materials is an important issue in the geological disposal of high-level radioactive waste. Among the materials for containers in the proposed Yucca Mountain (YM) repository, Ni-Cr-Fe-Mo and Ni-Cr-Mo alloys have been main candidates. One of them, Alloy 825, is the focus of this study. Containers will be made by welding plates both longitudinally and circumferentially. Currently, Alloy 22 is the main candidate material due to its superior corrosion resistance. Even in stabilized Ni-Cr-Fe-Mo alloys, such as Alloy 825, welding produces a heat affected zone in which grain boundary carbide precipitates and sensitization in a narrow region close to the fusion boundary may occur. Changes in material microstructure and microchemistry, particularly at grain boundaries, can affect mechanical properties due to thermal embrittlement or decrease in corrosion resistance as a result of sensitization.

Intergranular corrosion has been known to occur for Ni-Cr-Fe-Mo alloys in specific environments and can promote stress corrosion cracking and even disintegration at the grain boundary. It is generally accepted that the principal feature responsible for this phenomenon in stainless steels and Cr-bearing nickel alloys is the existence of a narrow chromium-depleted zone adjacent to carbide precipitates in the grain boundary region. Extensive research has been conducted

to quantify the grain boundary chemistry of stainless steels [1,2] and other Ni-Cr-Fe alloys such as Alloy 600.[3-6] However, very few studies exist in the literature on the development of chromium depletion during the sensitization of Alloy 825. Raymond [7] has conducted one of these studies on the mechanisms of sensitization and stabilization of Alloy 825. He found that the sensitivity to intergranular corrosion of Alloy 825 can be attributed to the precipitation of Cr-rich carbides and the formation of a Cr-depleted area adjacent to the grain boundary but no Cr concentration profile was experimentally measured. Thus, determination of the chemistry in the vicinity of grain boundaries is important in understanding the thermal stability of these alloys.

Energy dispersive X-ray spectroscopy with the analytical electron microscope (AEM) is one of the few techniques available for analysis of grain boundary chemistry. The development of the AEM with a finely focused electron probe has enabled sampling of very small volumes. Hall and Briant[1] have systematically determined the Cr distribution in the vicinity of carbides as a function of sensitization temperature and time in type 316LN austenitic stainless steels. Good agreement was found between the AEM measurements and the results calculated from thermodynamic models. Modeling of sensitization has been attempted both phenomenologically[8] and mechanistically.[9,10] Bruemmer[11] has reviewed the basic approaches to model sensitization. While phenomenological modeling is based on the normalization of bulk compositional effects on intergranular corrosion, mechanistic modeling considers the thermodynamics and kinetics of carbide precipitation and Cr depletion profile evolution. Numerous investigators [1-6] have attempted to predict the development of sensitization using these models. The success of these predictions was found to be dependent on

the selection of key parameters in the models such as activity coefficient, diffusion coefficient, and the critical values of Cr depletion for intergranular corrosion to occur.

In the study documented in this paper, a combination of corrosion tests and AEM measurements were employed to examine the factors affecting the sensitization of Alloy 825. Models predicting sensitization by taking into account interfacial Cr concentration and Cr depletion profile were correlated with experimental measurements.

II. EXPERIMENTAL PROCEDURES

Alloy 825, supplied by INCO Alloys International as a 12.5 mm thick plate in the hot-rolled and mill-annealed (MA) condition, was used in this study. Its chemical composition is given in Table I as Heat A. The microstructure of the as-received MA material was observed to have a dual grain size with areas of large grains surrounded by areas of very small grains.[12] Whereas the grain boundaries were found to be completely devoid of precipitates, a large number of small intragranular carbide precipitates and large cuboidal particles within some of the grains were observed in the MA microstructure. Specimens of Alloy 825 were solution-annealed (SA) at 1,200°C for 10 min followed by fast quenching in cold water. The high-temperature treatment produced significant grain growth and dissolution of the intragranular precipitates. The grain boundaries of the SA material were found to be free of precipitates.

Both MA and SA specimens were then heat treated at various temperatures ranging from 600 to 800°C for 0.1 to 1,000 hours and still-air cooled. All specimens were then subjected to the following corrosion tests: (1) ASTM A262 Practice C,[13] boiling 65 % HNO_3 for five 48 hours periods; (2) ASTM A262 Practice D,[13] boiling 50 % H_2SO_4 + 42 g/L $Fe_2(SO_4)_3$-$4H_2O$ for 120 hours; (3) ASTM G-61,[14] cyclic potentiodynamic polarization (CPP) at a potential scan rate of 0.167 mV/s in a 100 ppm Cl^- solution at 95°C. Both the nitric acid and CPP tests were performed using Heat A. The sulfuric acid - ferric sulfate tests were conducted using a 3.1 mm thick plate also obtained from INCO Alloys International. The composition of this plate is shown in Table I as Heat B. While the first two tests were used to evaluate the susceptibility to intergranular corrosion, the third test was undertaken to determine the repassivation potential (E_{rp}) for localized corrosion in a chloride-containing environment relevant to the proposed YM repository. Selected specimens were then cross-sectioned for metallographic observation.

AEM analyses were conducted to determine the composition of the grain boundary precipitates and the associated Cr depletion using a Phillips EM420 scanning transmission electron microscope (STEM). Thin-foil specimens were prepared by cutting slices about 1,000 μm thick from the heat-treated material followed by mechanical thinning to 40 μm. Discs 3 mm in diameter were then punched out and electropolished in a jet-polishing apparatus using a perchloric-ethanol mixture until a small perforation was detected. At least two specimens for each heat treatment condition were examined. The quantitative X-ray microanalyses were carried out using a 20 nm electron beam diameter. The X-ray intensities were converted to concentration of species using the Cliff-Lorimer procedure.[15] In this procedure, the ratio of concentration of species is assumed to be proportional

to the ratio of their X-ray intensities, because the X-ray fluorescence and absorption can be neglected due to the small thickness of the sample. The relationship can be expressed as:

$$\frac{C_{Cr}}{C_{Ni}} = k_{CrNi}\left(\frac{I_{Cr}}{I_{Ni}}\right) \quad (1)$$

where C_{Cr} and C_{Ni} refer to the concentrations of Cr and Ni, respectively, and I_{Cr} and I_{Ni} refer to their respective X-ray intensities. The factor, k_{CrNi}, is calculated by conducting the analysis at a location remote from the grain boundary and using the known bulk chemical composition of the alloy as reference. Nickel, the main alloying element in Alloy 825, was used as the basis for calculating the concentration of other alloying elements. Since in this investigation the characteristic intensity peaks of the desired elements are far apart, the errors in concentrations were estimated from replicate measurements rather than by the sum of relative errors (95 percent confidence interval/average value) of k and I values as used by Goldstein and Williams.[15] The standard deviation (σ) for the measurement of Cr concentration was estimated to be 0.5 at. % and for Mo about 0.16 at. %.

III. EXPERIMENTAL RESULTS

A. Intergranular Corrosion Tests

According to ASTM A-262-93a, Standard Practice C, the evaluation of the susceptibility to intergranular corrosion is made by calculating an average corrosion rate over the five 48 hours test periods. In order to compare the data for different conditions, corrosion rates were normalized by

dividing the corrosion rate of the heat-treated specimens by that of the MA (0.107 mm/yr for Heat A) and SA (0.116 mm/yr for Heat A and 0.100 mm/yr for Heat B) specimens, respectively. It has been previously reported that sensitization of the thermally treated SA specimens was observed to occur more readily than that of the MA specimens.[12] The normalized corrosion rates for the thermally treated SA specimens of Heat A are shown in Figure 1. It can be seen that specimens heat treated at 700°C exhibited the highest corrosion rates for both time periods of 15 and 100 hours. The corrosion rate increased with increasing heat treatment time for the lower aging temperatures of 600, 640, and 700°C, whereas a decrease was observed for the higher aging temperatures of 750 and 800°C. The corrosion rate is calculated as uniform dissolution regardless of the localized morphology of the attack following the procedures of the ASTM Standard. However, cross sections of the specimens indicated the development of localized dissolution along the grain boundaries in the form of intergranular corrosion. The extent of localized dissolution was also found to be greater for the heat-treated SA specimens compared to the heat-treated MA specimens. No signs of localized attack were detected in the SA specimen without additional thermal treatment.[12]

Results of the sulfuric acid-ferric sulfate tests using Heat B are shown in Figure 2. It is clearly seen in Figure 2 that the maximum corrosion rate was observed in the specimen heat treated for 1,000 hours at 640 °C. From Figures 1 and 2, it is apparent that the nitric acid test is much more sensitive to grain boundary precipitation than the sulfuric acid-ferric sulfate test even though different specimen heats were employed. The differences in the corrosion rates observed in these tests are the result of the different sensitivities of these tests to grain boundary chemistry, as discussed by Streicher.[16] The sulfuric acid-ferric sulfate test is sensitive to the extent of the Cr-depletion region,

both measured by its microstructural width and its minimum Cr concentration. The nitric acid test is sensitive to Cr depletion, the precipitation of σ-phase, and the presence of Cr^{6+} species in the test solution. For sensitized microstructures that do not contain σ-phase, the higher Cr-containing phases, such as chromium carbide precipitates at the grain boundaries, have higher corrosion rates in nitric acid solutions containing Cr^{6+}. If the grain boundary region has some level of Cr depletion as a result of sensitization, preferential corrosion occurs initially in this region in nitric acid. Once a sufficient concentration of Cr^{6+} species is generated, accelerated corrosion occurs in the grain boundary where there is an enriched Cr phase. The relatively low corrosion rate in sulfuric acid-ferric sulfate solution seems to indicate a very narrow region of Cr depletion. This finding is in agreement with previous results reported by Brown [17] for Alloy 825 with a higher carbon content (0.03 %) and slightly lower Cr concentration (21.24 %).

A convenient method for displaying the data of the intergranular corrosion tests is the use of the time-temperature-sensitization (TTS) diagram. The results for both heat-treated MA and SA specimens from Heat A are shown in Figure 3. A value of 0.3 mm/yr was adopted as a boundary between the sensitized and the nonsensitized regions of the diagram based on the previous work of Raymond.[7] It should be emphasized, however, that the location of the boundary depends on the solution composition and other environmental conditions that are used to perform the test (in this case, ASTM A-262, Practice C). In a different environment, the sensitization domain may be reduced or extended beyond that shown in Figure 3.

The effect of sensitization on localized corrosion of Alloy 825 was examined by measuring the repassivation potential, E_{rp}, in a 100 ppm Cl^- solution at 95°C using CPP tests. The correlation between the corrosion rate in the nitric acid test and the repassivation potential in chloride solution is shown in Figure 4 as functions of sensitization temperature and time. As shown in Figure 4, a good correlation exists between the E_{rp} measured in the chloride solution and the corrosion rate in boiling nitric acid. The maximum corrosion rates observed in the specimens heat treated at 700°C coincide with the minimum E_{rp} values for both aging time periods of 15 and 100 hours. Heat-treatment conditions that created a sensitized microstructure also resulted in a significant decrease in E_{rp}, indicating that the sensitized microstructure is less resistant to localized corrosion. Localized corrosion in the form of pitting was observed to occur preferentially along the grain boundaries.[12]

B. Grain Boundary Precipitation

Grain boundary precipitation was observed at all heat treatment temperatures and times employed in this study. The microstructures of the grain boundary regions of the heat-treated Alloy 825 Heat A are shown in Figures 5 through 8 for different aging conditions. The TEM images in Figures 5 through 8 correspond to various aging time periods at 640, 700, 750, and 800°C, respectively. Electron diffraction analysis of the grain boundary precipitates confirmed that the crystal structure was $M_{23}C_6$-type carbide within an austenitic matrix oriented to a [001] zone axis, as shown in the diffraction pattern insert in Figure 7a. The globular $M_{23}C_6$-type carbide precipitates observed in this study are similar to those previously reported for this alloy.[7] The chemical composition of the grain boundary carbides measured in thin-foil specimens is presented in Table II for two

electropolishing solutions. Surface chemistry artifacts in Alloy 825 and variations of the grain boundary chemistry in relation to the electrolytes used for electropolishing were observed. The chromium content of the carbides for the perchloric acid-polished specimens is substantially higher than that for the nitric acid-polished specimens and consistent with previous findings.[1,18] Whereas $M_{23}C_6$ carbide precipitates in type 316LN stainless steels had about 65 wt. % Cr,[1] those in Alloy 825 can be up to 75 wt. % Cr.[18] A detailed discussion concerning the effect of electropolishing in nitric acid solution has been published elsewhere.[19]

The effect of heat treatment temperature and time on grain boundary precipitation is also clearly shown in Figures 5 through 8. It was observed that the size of the carbide precipitates increases with increasing aging temperature; however, their density decreases significantly. A low aging temperature of 640°C produced finer, but more numerous, grain boundary precipitates (Figure 5). The size of precipitates increased substantially upon aging at 800°C (Figure 8). A similar trend was also observed regarding the effect of aging time as revealed in Figure 5 for three different aging periods. The precipitate morphology after a 1,000-hour treatment at 640°C became coarse and discrete, quite different from that corresponding to aging for shorter times.

C. Chromium Depletion Profiles

Chromium depletion profiles were obtained across grain boundaries between precipitates. Several grain boundary areas were examined on duplicate specimens with the same treatment. Figures 9 through 12 show representative profiles for 640, 700, 750, and 800°C, respectively, at

various aging times. The minimum of the grain boundary Cr concentrations are listed in Table III for the same thermal treatments. Significant chromium depletion occurred for most of the time/temperature combinations employed. A pronounced Cr depletion was observed at 700°C, and also at lower temperatures for the most prolonged treatments. Variations in the Cr concentration profiles due to preferential electropolishing were also observed during TEM thin-foil specimen preparation of Alloy 825 using nitric acid and perchloric acid solutions. The Cr-depleted zone observed in specimens electropolished in perchloric acid solution was found to be significantly deeper and wider than that in specimens electropolished in nitric acid solution. [19]

A significant effect of aging time on the grain boundary depletion of Cr was also observed. For an aging temperature of 700°C, while longer aging time did not appreciably affect the minimum Cr concentration (Table III), a widening of the depleted zone is noted in Figure 10. However, at 800°C, while the minimum Cr concentration slightly increased with increasing aging time, the depletion width decreased slightly, as shown in Figure 12. An intermediate behavior without an apparent change in both the width of the depleted zone and the minimum Cr concentration, is noted at 750°C (Figure 11). Contrary to the high aging temperature, at 640°C the minimum Cr concentration gradually decreased with increasing time, while the depletion width increased (Figure 9). The effect of aging temperature on the grain boundary depletion of Cr is shown in Figures 13 and 14 for aging times of 15 and 100 hours, respectively. In both time periods aging at 700°C produced the lowest grain boundary Cr concentration, and aging for 100 hours resulted in the widest depletion.

In some specimens, Mo depletion was also observed, but the observations were not entirely consistent. It is possible that the small concentration of Mo present in the alloy did not permit an accurate analysis of the profile with the instrument used in this investigation. The relative error in the determination of the Mo content in the matrix is close to 30 %. It must be noted, however, that carbide precipitates consistently exhibited higher Mo contents than the matrix.

IV. DISCUSSION

A. Kinetics of Sensitization

The results of this study essentially confirm the findings reported by Raymond [7] regarding the temperature range for sensitization and the location of the "nose" in the TTS diagram for Alloy 825. The thermally treated SA material exhibited a much higher degree of sensitization than that of the MA material. This was rationalized by Raymond in terms of the redissolution of matrix $M_{23}C_6$ carbides with the resulting increase in the soluble carbon content of the matrix and reprecipitation of these carbides along the grain boundaries. However, for a material solution-annealed at 1,204°C and then heat-treated at 940°C for 1 hour (temperature of the current stabilizing treatment for MA samples), Raymond found a much larger sensitization domain, in terms of time and temperature, than that found in the current investigation. The simplest explanation for the greater degree of sensitization of the material studied by Raymond is related to the higher carbon content of the original composition of Alloy 825. Raymond tested a heat with a carbon content of 0.03 wt. %, whereas the heat used in the present study contained only 0.01 wt. %. The effect of the

higher carbon content on the sensitization of Alloy 825 is understandable in terms of chromium depletion as determined by the equilibrium chromium concentration at the carbide–matrix interface.

From the corrosion rates of the SA specimens heat treated for 15 hours at temperatures ranging from 600 to 700°C, an activation energy of approximately 292.6 kJ/mole was calculated by plotting corrosion rates as a function of the reciprocal of temperature. This value is relatively close to the activation energy for matrix diffusion of chromium in nickel-based alloys such as Alloy 600 (Ni-15%Cr-6%Fe) which is 277.7 kJ/mole[20] and Alloy 800 (32%Ni-21%Cr-45%Fe) with a value of 287.4 kJ/mole.[21] Data for binary Ni-Cr alloys reported by Pruthi et al.[20] also indicate that the activation energy increases with increasing chromium content, reaching about 290.4 kJ/mole for Ni-29.7%Cr. This effect of the chromium content on the activation energy for chromium diffusion may be the reason of the value for the activation energy obtained in the present study, since the chromium content of Alloy 825 is comparable to that of Alloy 800. It appears that the corrosion rates measured in the thermally-treated SA samples can be related, at least qualitatively, to the degree of sensitization, as given by the level of chromium depletion and the width of the depleted zone. The width of the depleted zone is proportional to $2(Dt)^{1/2}$, where D is the matrix diffusion coefficient of chromium at the temperature of interest and t is time. The activation energy and preexponential factors for Cr diffusion in Alloy 825, adopted from the study by Paul et al., [21] are 287.4 kJ/mol and 3.24 cm^2/s, respectively. Chromium depletion width can be estimated assuming a critical Cr level of 21 at. % as compared to the 24.6 at. % for the Cr content in the bulk. Figure 15 shows a comparison of measured depletion zone widths with the calculated results for various temperatures. The

calculation generally predicts depletion zone widths for the heat treatments used in this study with the exception of 800°C, temperature at which significant Cr replenishing takes place in a short time.

The high activation energy for Cr diffusion indicates a very strong temperature dependence. A decrease in temperature from 600 to 400°C implies a decrease of at least five orders of magnitude in the rate of the controlling process if there is no change in the mechanism with respect to that prevailing in the 600 to 700°C range. This implies that heat treatments extended for more than 18 years will be required at 400°C to obtain the degree of sensitization observed in the high-temperature range. In order to study the thermal stability of Alloy 825 at temperatures closer to those expected under repository conditions within a realistic time frame, it would be necessary to enhance metallurgical processes responsible for sensitization, such as carbide precipitation and chromium diffusion. This may be accomplished by introducing a higher dislocation density in the γ-phase matrix of SA samples through cold work prior to the sensitization treatments. Park et al.[22] found that cold work preceding heat treatment accelerates the precipitation of M_7C_3 carbides in Alloy 600. The effect of cold work on thermal stability is also important from a practical point of view. Surface and near-surface areas of the high-level radioactive waste containers could be affected by cold work arising from sudden mechanical loads, impingement by wall-rock shear offsets, and other interactions leading to localized plastic deformation. Initial investigations using U-bend specimens of SA material, however, did not indicate any effect of cold work on sensitization kinetics.[23] This may indicate that the amount of cold work in the U-bend was inadequate or sensitization of Alloy 825 is relatively insensitive to prior cold work.

B. Modeling of Grain Boundary Chemistry

Modeling of Cr depletion kinetics in single phase fcc Ni-Cr-Fe alloys has been attempted by numerous investigators and reviewed by Bruemmer.[11] The formation of $M_{23}C_6$ carbide which is the prevailing carbide in most of these alloys, is represented by the following overall reaction:

$$\mathbf{M_{23}C_6 \rightleftarrows 23\ M + 6\ C} \tag{2}$$

where M is mostly Cr, but may contain some Mo, Ni, and Fe. The equilibrium constant for this reaction, that decreases with decreasing temperature [11], is written as:

$$\mathbf{K = \exp\left(-\frac{\Delta G}{RT}\right) = \frac{a_{M_{23}C_6}}{(a_M)^{23}(a_C)^6}} \tag{3}$$

Since the activity of the carbide can be assumed to be equal to 1 under standard conditions, a higher carbon content in the alloy implies a lower chromium activity or concentration at the interface. The activities in Eq. (3) can be written in terms of the appropriate concentrations as:

$$\mathbf{a_{Cr^*} = \gamma_{Cr^*} X_{Cr^*};\ a_c = \gamma_c X_c} \tag{4}$$

where the M is replaced by an equivalent Cr concentration, Cr*, that includes the effect of Mo. The γs are the activity coefficients, and the Xs are the concentrations of the corresponding elements. The activity coefficient of carbon in solid-solution has been reviewed by Hillert and Qui[24] and Natesan and Kassner.[25] The activity coefficient for Cr can be calculated either by the approach of the pairwise

interaction parameters as given by Was and Kruger[3] or by using empirical equations as employed by Bruemmer.[11]

The minimum Cr concentration in Alloy 825 was calculated using the value for the equilibrium constant from the work by Richardson.[26] The value for the activity coefficient of carbon was calculated using the formulation of Natesan and Kassner.[25] Insufficient information is available for determining the activity coefficients for chromium. Activity coefficients were estimated on the basis of the Cr activity vs. temperature equation given by Bruemmer,[11] adjusted by using the interfacial concentration measured at 600 °C. Figure 16 compares the measured Cr minimums with the calculated values as a function of temperature. A good agreement between the calculated results and the measurements is found for all aging temperatures with the exception of specimens treated at 640 °C for 15 and 100 hours. It is apparent that equilibrium was not reached for these heat treatment times, although it occurred in 1,000 hours. Another possible reason for this discrepancy may be the morphology of carbides in the specimens aged at lower temperatures. The carbides were small, and more continuously distributed along the grain boundaries. Hence, it was difficult to find a grain boundary area devoid of precipitation in order to determine accurately the interfacial Cr concentration. The electron beam partially intersected the overlying carbides affecting the results of the chemical analysis. Data for $M_{23}C_6$ carbides indicate that the equilibrium Cr concentration at the matrix-carbide interface decreases with decreasing temperature.[11] The experimental results shown in Figure 16 are consistent with this prediction over the temperature range of 800 to 600°C.

Whereas the chromium concentration at the carbide/matrix interface is thermodynamically determined, the profile of the chromium concentration gradient is dominated by diffusional factors. The depletion zone width has been predicted to increase with aging temperature from 600°C to 700°C for both austenitic stainless steel ($M_{23}C_6$carbides)[11] and Alloy 600 (M_7C_3 carbides)[3]. Beyond this temperature, the depletion zone width increases, but the minimum Cr concentration also increases. Thus, the total volume of depleted material below a certain critical Cr concentration decreases. These predictions are essentially confirmed by the present set of experiments.

Modeling of chromium concentration profiles was performed based on the equations given by Hall and Briant.[1] The minimum Cr content for each calculated profile was chosen to match the experimental measurement, rather than the calculated equilibrium value. The calculated profiles for Alloy 825 annealed for 15 hours at various temperatures are presented in Figure 17. The calculated profiles at 700°C are shown in Figure 18 superimposed on the experimental data. The model seems to not fully account for the broadening of the Cr depleted region after long aging times. The discrepancies may be attributed to the diffusion coefficient values chosen for the calculations. The effect of increasing the diffusion coefficient is shown in Figure 19 for the specimen aged at 700°C for 15 hours. The Cr depletion width from the experimental data is in agreement with that of the calculated profile using a diffusion coefficient an order of magnitude larger than the literature value.[21]

C. Grain Boundary Chemistry and Intergranular Corrosion

The effects of heat treatment temperature and time on corrosion rates in boiling 65 % nitric acid may be better understood if combined with the results of the STEM analyses. For this purpose, the size of the chromium depletion zone and the level of Cr were considered together as an equivalent Cr depletion zone width, as suggested by Was et al.[27] The area of the depletion profiles below various Cr concentrations was calculated. This area was then divided by the bulk Cr concentration to obtain an equivalent width of the Cr depletion zone (in nanometers). The corrosion rate in boiling 65 % nitric acid is plotted as a function of the equivalent Cr depletion size for various Cr levels in Figure 20. A good correlation was obtained between the corrosion rate and depletion size below a Cr concentration of 21 at. %, suggesting that the corrosion rate is determined by the size of the depletion zone below a critical Cr concentration of about 21 at. % (about 19 wt. %). In contrast, the corrosion rate in boiling nitric acid did not correlate well with the minimum Cr concentration at the grain boundaries. For example, both aging treatments at 700°C, for 15 and 100 hours, showed the same minimum Cr concentration, but the latter treatment resulted in significantly higher sensitization as measured in the nitric acid test.

The effect of Cr depletion zone size on the E_{rp} is shown in Figure 21. The correlation is not as good as that for the corrosion rate in nitric acid. This poorer correlation presumably arises from the fact that localized corrosion resistance is a function of both Cr and Mo. The STEM analyses of Mo did not indicate significant depletion, although the carbide analyses showed higher Mo. This observation may be due to a lack of resolution of the Mo analyses, low Mo concentrations, or the

result of a very narrow Mo profile. Another possibility is that a linear correlation of Cr depletion to E_{rp} is not valid. It can be observed in Figure 21 that below a depletion zone size of about 5 nm, the E_{rp} levels off, indicating that pitting takes place mostly in the matrix.

Sensitization of Alloy 825 may be initiated during either fabrication from plates or closure welding of containers. Annealing of both types of welds may be possible. The closure weld must be annealed in a manner whereby the temperature of the contained spent fuel assemblies is maintained below 350°C. The advanced conceptual design for the proposed YM repository includes a thick steel outer disposal overpack. The heat generated during the welding closure of the outer disposal overpack may also induce growth of any grain boundary precipitates and the concurrent increase in the width of the associated Cr-depletion zones. Depending on the thermal loading of the repository, sensitization may continue after final disposal. The results of E_{rp} measurements on sensitized Alloy 825 confirm that the existence of Cr-depletion zones decreases the resistance of the material to localized corrosion in a potential repository environment. While the presence of a thick steel overpack may galvanically protect the Alloy 825 inner disposal overpack from localized corrosion even after the outer barrier is breached, it is apparent that the Cr-depletion zones and carbide precipitates may act as local anodes and undermine the integrity of the waste package.

V. CONCLUSIONS

The following conclusions can be drawn from this investigation:

1. Alloy 825 with a very low carbon content (~0.01 wt %) is still susceptible to sensitization. Both grain boundary $M_{23}C_6$ precipitation and significant chromium depletion in the vicinity of the carbides are present for all heat treatment temperatures ranging from 600 to 800°C.
2. The effects of heat treatment on chromium depletion profiles are related to the development of the sensitization process. The most severe sensitization was observed after aging at 700°C for 100 hours. Contrary to the progressive severity of sensitization with time at low temperatures, replenishing of the depleted region was observed to occur for high temperature heat treatments.
3. The nitric acid test was found to be much more sensitive to grain boundary chemistry than the sulfuric acid-ferric sulfate test. The observed differences in the corrosion rates of the sensitized Alloy 825 can be attributed to preferential intergranular corrosion as a result of microchemistry variations in the grain boundary region. Sensitization prompts localized corrosion along grain boundaries and decreases E_{rp} in chloride containing solutions.
4. The degree of sensitization in Alloy 825 was quantified and correlated well with the corrosion test results in boiling nitric acid using an equivalent chromium depletion zone size below a chromium concentration of 20–21 at. %. Model predictions are strongly dependent on the selection of key modeling parameters.
5. The sensitization process was found to be strongly dependent on temperature, with an apparent activation energy of approximately 292 kJ/mole in the 600 to 700°C range, which indicates that very prolonged heat treatment are required to induce sensitization at lower temperatures.

ACKNOWLEDGMENTS

The authors wish to thank Messrs. W. J. Machowski and H. G. Saldana for conducting corrosion experiments and TEM specimen preparation. This paper was prepared to document the work performed at the Center for Nuclear Waste Regulatory Analyses (CNWRA) for the U.S. Nuclear Regulatory Commission (NRC), Office of Nuclear Materials Safety and Safeguards, Division of Waste Management, under Contract No. NRC-02-97-009. This paper is an independent product of the CNWRA and does not necessarily reflect the views or the regulatory position of the NRC.

REFERENCES

1. E. L. Hall and C. L. Briant: Metall. Trans., 1984, vol. 13A, pp. 793-811.
2. S. M. Bruemmer and L. A. Charlot: Scripta Met., 1986, vol. 20, pp. 1019-1024.
3. G. S. Was and R. M. Kruger: Acta Metall., 1985, vol. 33, pp. 841-854.
4. G. S. Was: Corrosion,1990, vol. 46, pp. 319-330.
5. E. L. Hall and C. L. Briant: Metall. Trans., 1985, vol. 16A, pp. 1225-1236.
6 J. J. Kai, G. P. Yu, C. H. Tsai, M. N. Liu, and S. C. Yao: Metall. Trans., 1989, vol. 20A, pp. 2057-2067.
7. E. L. Raymond: Corrosion, 1968, vol. 24, pp. 180-188.
8. V. Cihal: Intergranular Corrosion of Cr-Ni Stainless Steel, Unieux Conference, 1969.
9. C. Stawstrom and M. Hillert: J. Iron Steel Inst., 1969, vol. 207, pp. 77-85.
10. C. S. Tedmon, Jr., D. A. Vermilyea, and J. H. Rosolowski: J. Electrochemical Soc., 1969, vol. 118, pp. 192- 202.
11. S. M. Bruemmer: Corrosion, 1990, vol. 46, pp. 698-709.
12. G. Cragnolino and N. Sridhar: Long Term Stability of High-Level Nuclear Waste Container Materials: I - Thermal Stability of Alloy 825, Center for Nuclear Waste Regulatory Analyses, CNWRA 93-003, San Antonio, TX, 1993.
13. American Society for Testing and Materials. Standard A 262-93a, ASTM Annual Book of Standards, vol. 3.02, ASTM, Philadelphia, PA, 1993, pp. 1-16.
14. American Society for Testing and Materials. Standard G 61, ASTM Annual Book of Standards, vol. 3.02, ASTM, Philadelphia, PA, 1993, pp. 231-235.

15. J. I. Goldstein and D. B. Williams: Quantitative Microanalysis with High Spatial Resolution, The Metals Society, London, 1981, p.5.

16. M. A. Streicher: Intergranular Corrosion of Stainless Alloys, ASTM STP 656, American Society for Testing and Materials, Philadelphia, PA, 1978, p. 3.

17. M. H. Brown: Corrosion, 1969, vol. 25, pp. 438-443.

18. M. A. Shaikh, M. Iqbal, M. Ahmad, J. I. Akhtar, and K. A. Shoaib: J. Mater. Sci. Lett., 1992, vol. 11, p.1009.

19. Y.-M. Pan, N. Sridhar, D. S. Dunn, and G. A. Cragnolino: J. Mater. Sci. Lett., 1996, vol. 15, pp. 522-524.

20. D. D. Pruthi, M. S. Anand, and R. P. Agarwala: J. Nucl. Mater., 1977, vol. 64, pp. 206-210.

21. A. R. Paul, K. N. G. Kaimal, M. C. Naik, and S. R. Dharwadkar: J. Nucl. Mater., 1994, vol. 217, pp. 75-81.

22. J. M. Park, W. S. Ryu, and Y. H. Kang: J. Nucl. Mater., 1994, vol. 209, pp. 221-225.

23. N. Sridhar, G. Cragnolino, and D. S. Dunn: Experimental Investigation of Failure Processes of High-Level Nuclear Waste Container Materials, Center for Nuclear Waste Regulatory Analyses, CNWRA 95-010, San Antonio, TX, 1995.

24. M. Hillert and C. Qiu: Metall. Trans., 1991, vol. 22A, pp. 2187-2198.

25. K. Natesan and T. F. Kassner: Metall. Trans., 1973, vol. 4, pp. 2557-2566.

26. F. D. Richardson: J. Iron Steel Inst., 1953, vol. 175, pp. 33-51.

27. G. S. Was, H. H. Tischner, and R. M. Latanision: Metall. Trans., 1981, vol. 12A, pp. 1397-1408.

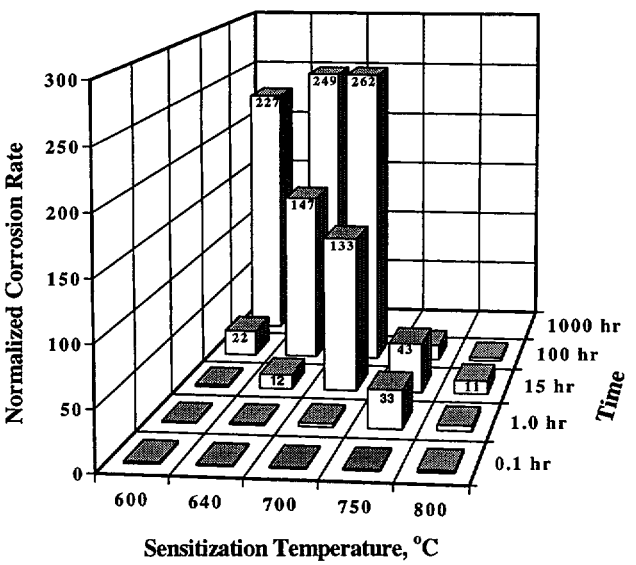

Figure 1. Effect of heat temperature and time on the corrosion rate of solution-annealed specimens of Alloy 825 (Heat A) in boiling 65 % nitric acid.

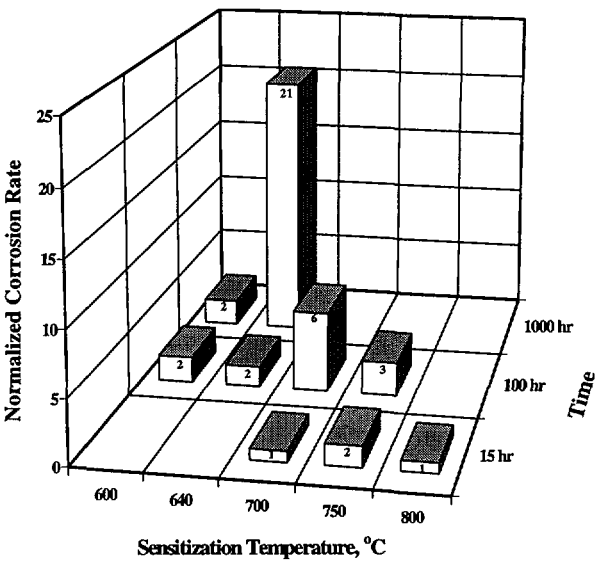

Figure 2. Effect of heat treatment temperture and time on the corrosion rate of solution-annealed specimens of Alloy 825 (Heat B) in boiling sulfuric acid plus ferric sulfate.

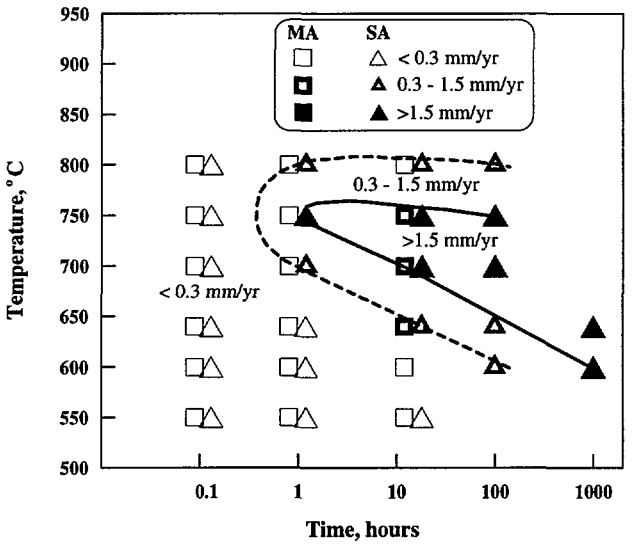

Figure 3. Time-temperature-sensitization diagram for heat treated mill-annealed and solution-annealed Alloy 825 specimens (Heat A). Corrosion rates determined in boiling 65 % nitric acid.

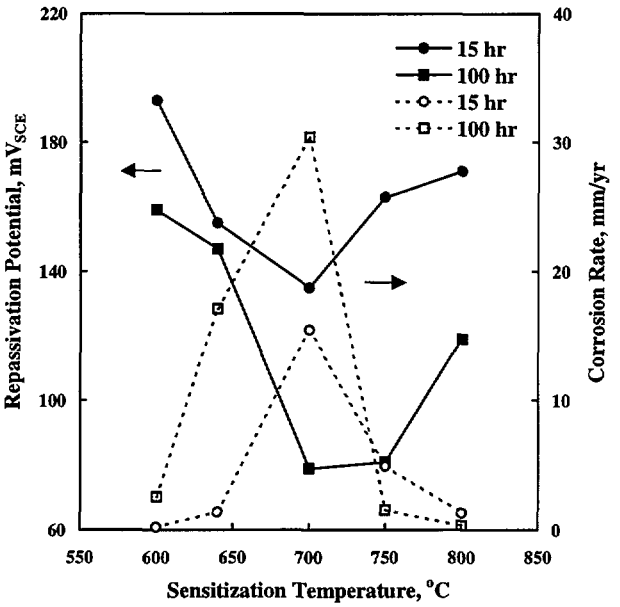

Figure 4. Comparison of the repassivation potential (in solid lines), E_{rp}, measured at a scan rate of 0.167 mV/s, in a 100 ppm chloride solution at 95 °C and the corrosion rate (in dashed lines) in 65 % nitric acid, for specimens of Heat B.

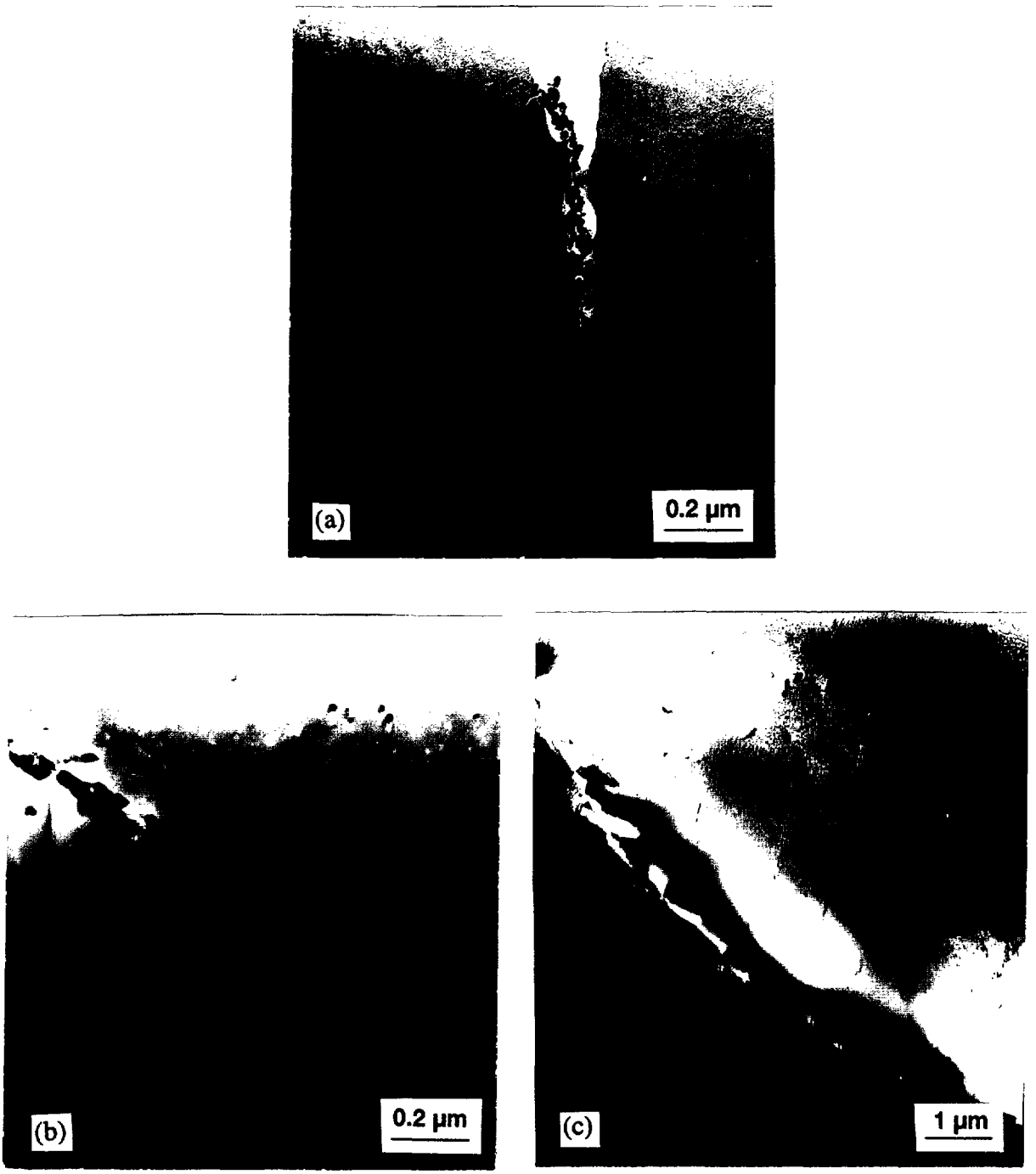

Figure 5. Transmission electron microscopy images of Alloy 825 solution annealed and heat-treated at 640 °C for (a) 15 hours, (b) 100 hours, and (c) 1,000 hours.

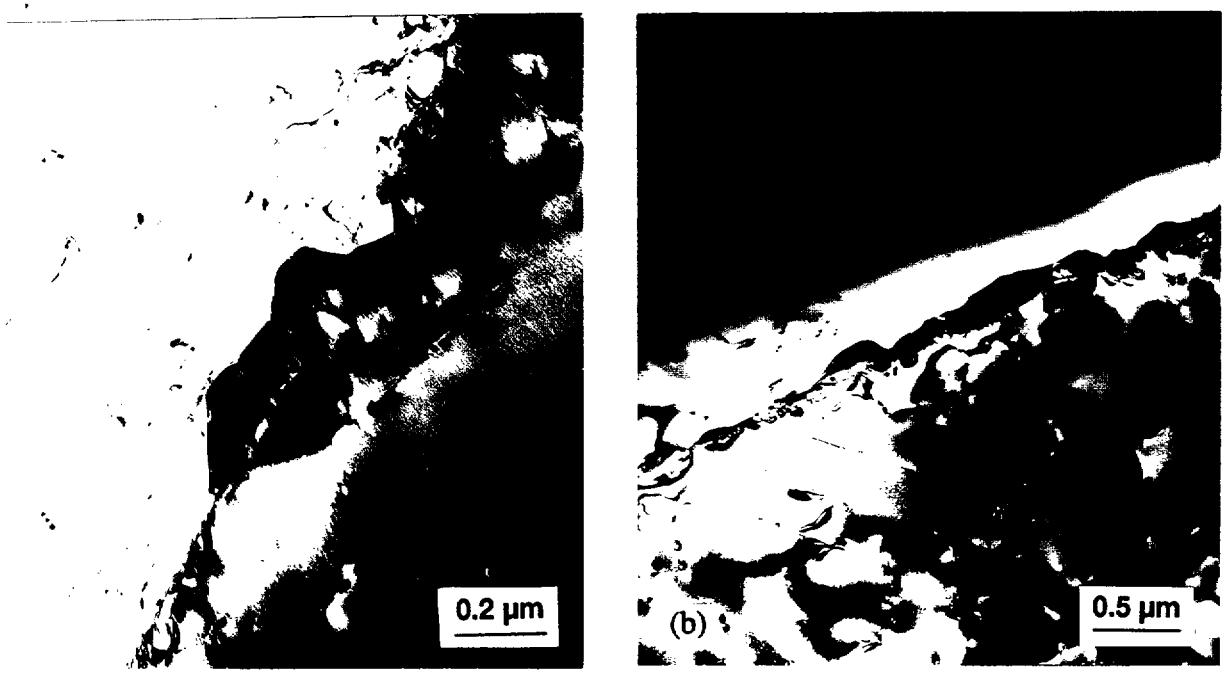

Figure 6. Transmission electron microscopy images of Alloy 825 solution annealed and heat-treated at 700°C for (a) 15 hours and (b) 100 hours.

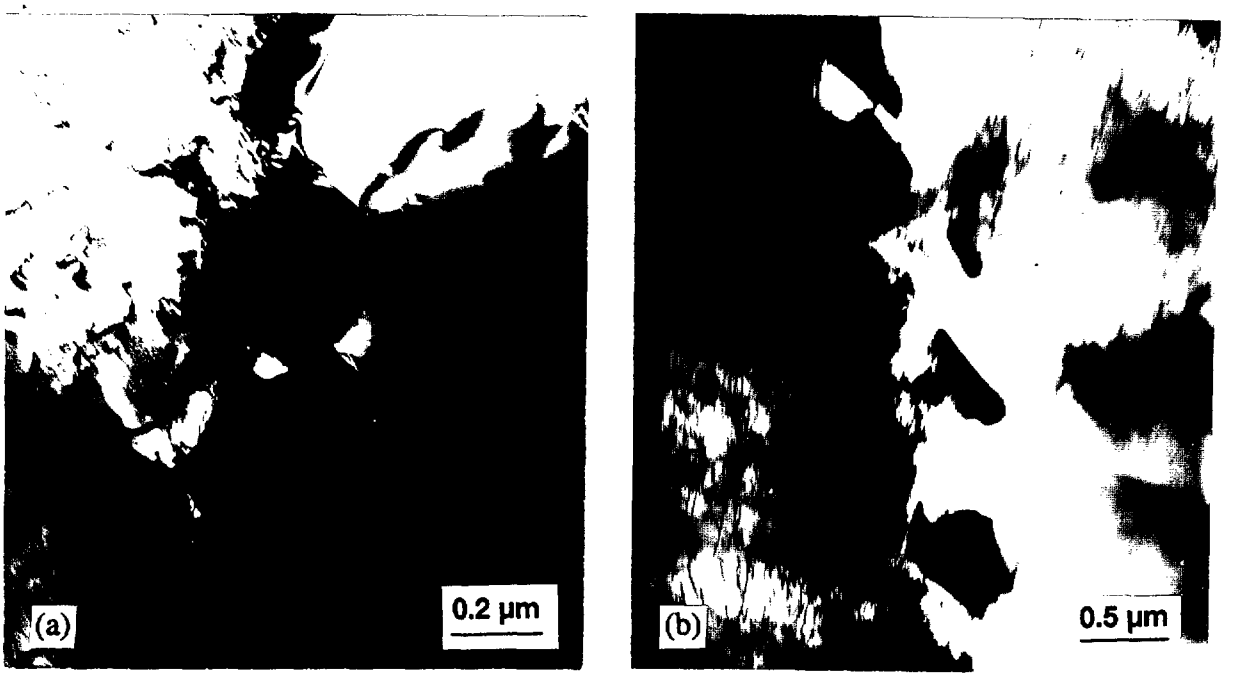

Figure 7. Transmission electron microscopy images of Alloy 825 solution annealed and heat-treated at 750°C for (a) 15 hours and (b) 100 hours.

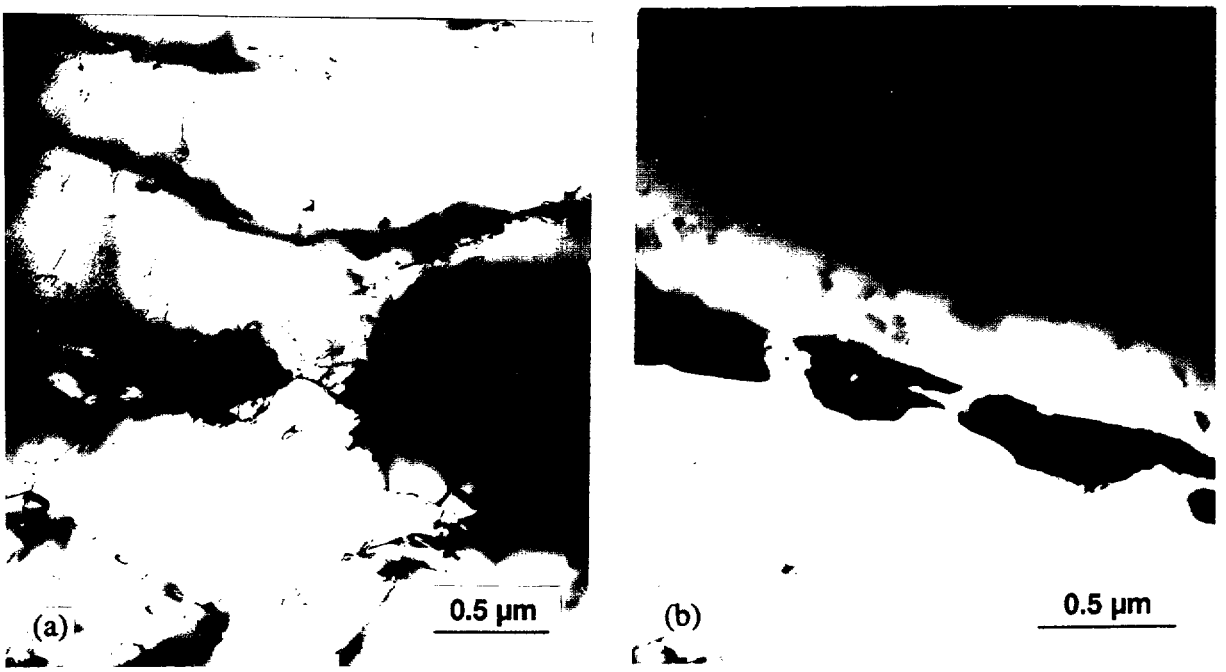

Figure 8. Transmission electron microscopy images of Alloy 825 solution annealed and heat-treated at 800 °C for (a) 15 hours and (b) 100 hours.

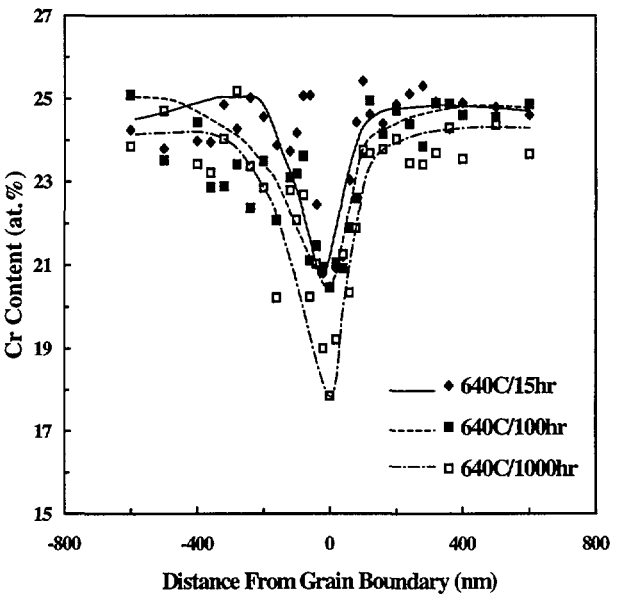

Figure 9. Chromium concentration profiles along a grain boundary of Alloy 825 containing $M_{23}C_6$ precipitates after heat-treated at 640 °C for various time periods.

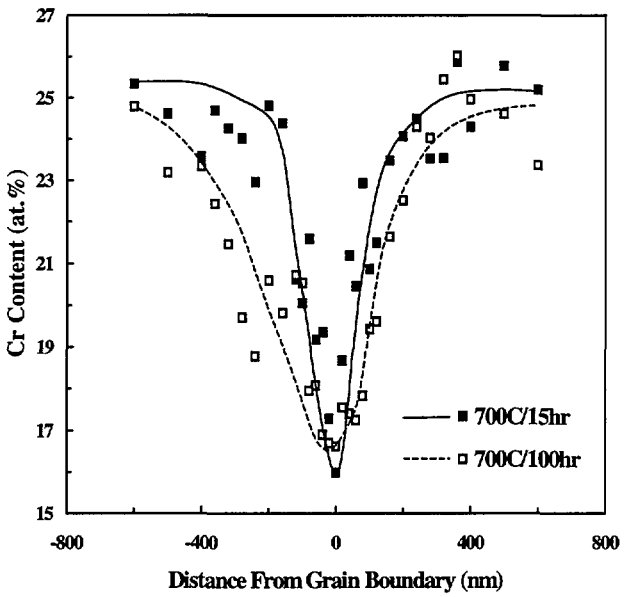

Figure 10. Chromium concentration profiles along a grain boundary of Alloy 825 containing $M_{23}C_6$ precipitates after heat-treated at 700 °C for various time periods.

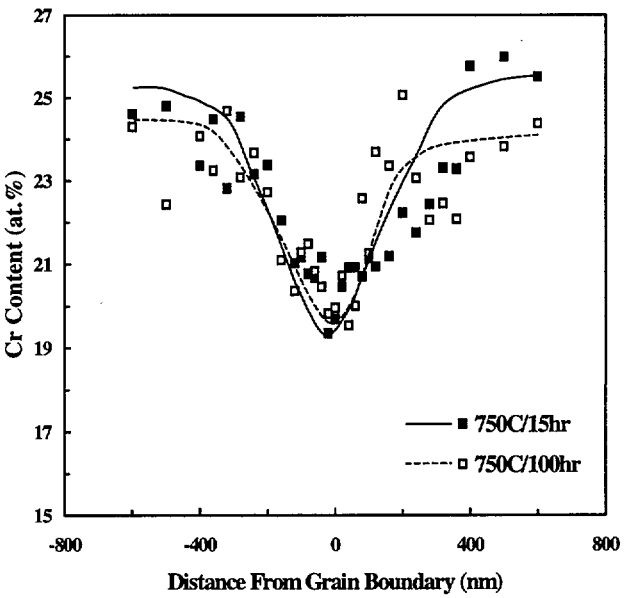

Figure 11. Chromium concentration profiles along a grain boundary of Alloy 825 containing $M_{23}C_6$ precipitates after heat-treated at 750 °C for various time periods.

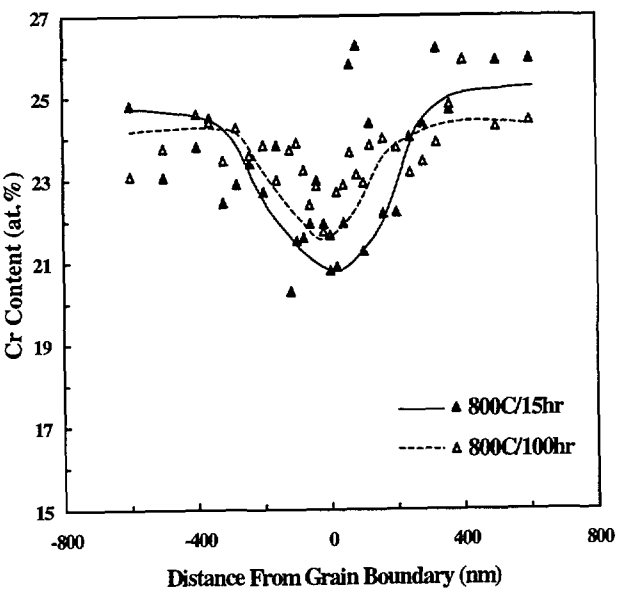

Figure 12. Chromium concentration profiles along a grain boundary of Alloy 825 containing $M_{23}C_6$ precipitates after heat-treated at 800 °C for various time periods.

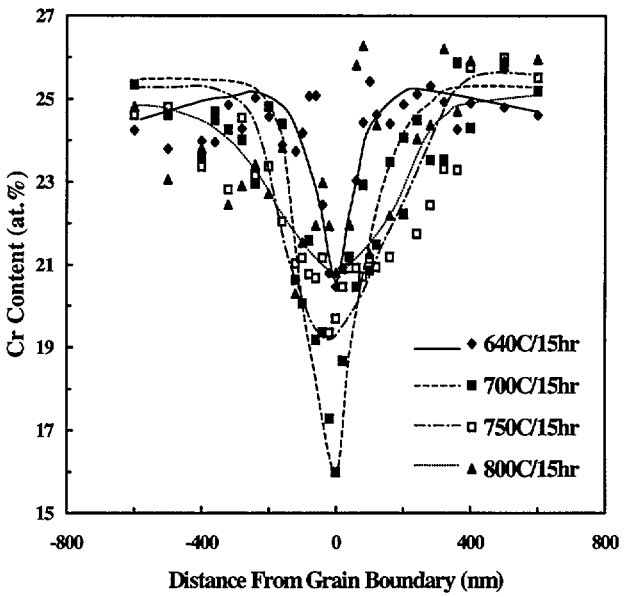

Figure 13. Chromium concentration profiles along a grain boundary of Alloy 825 containing $M_{23}C_6$ precipitates after heat-treated for 15 hours at various temperatures.

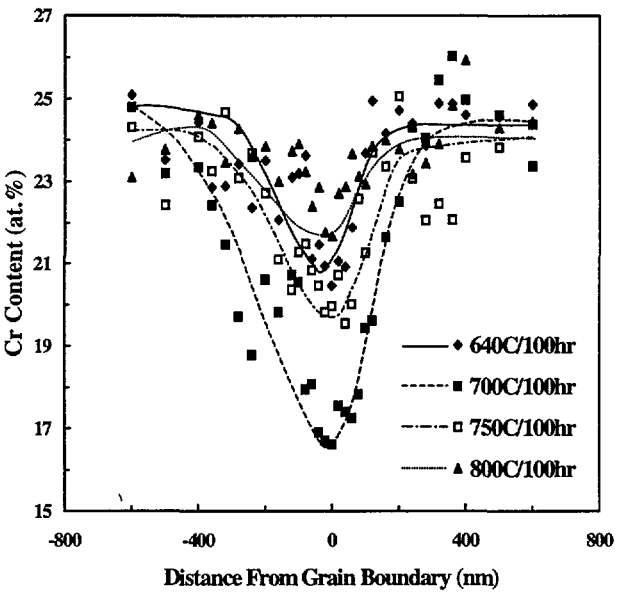

Figure 14. Chromium concentration profiles along a grain boundary of Alloy 825 containing $M_{23}C_6$ precipitates after heat-treated for 100 hours at various temperatures.

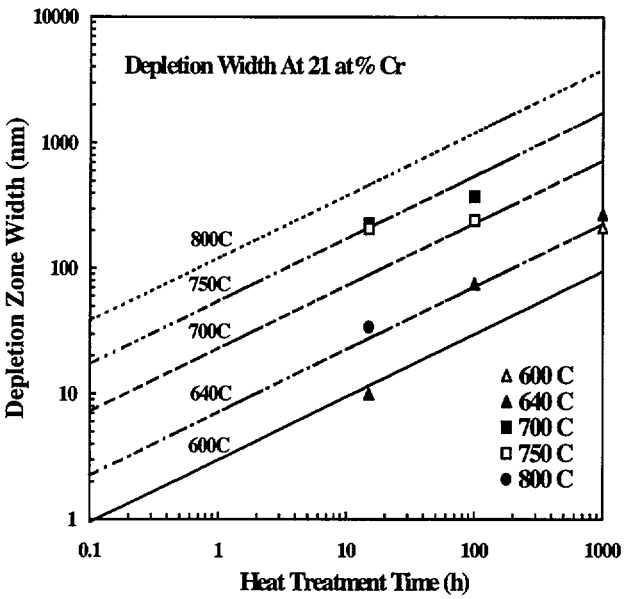

Figure 15. Comparison of measured and calculated chromium depletion widths.

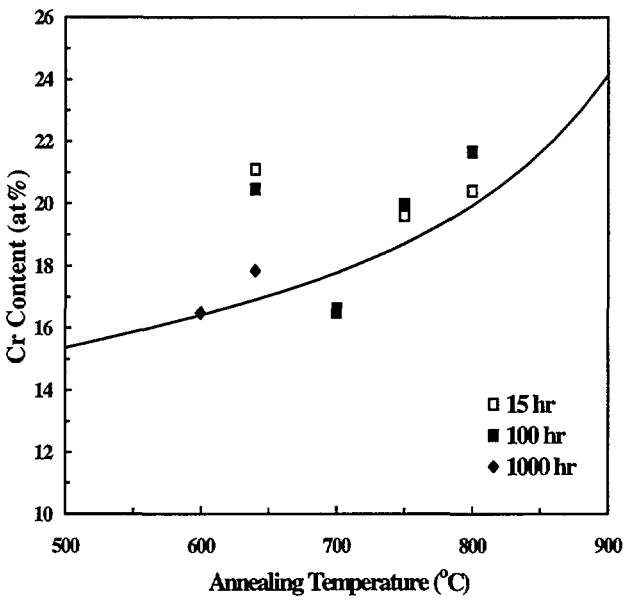

Figure 16. Comparison of measured and calculated chromium minimums.

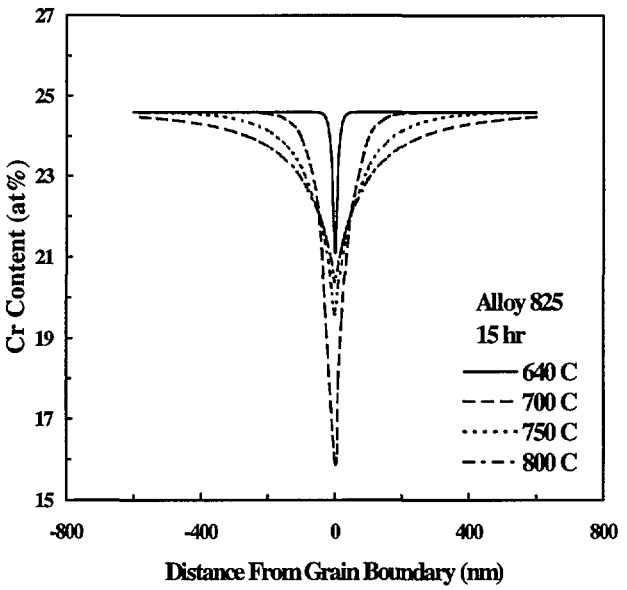

Figure 17. Calculated chromium concentration profiles for Alloy 825 heat-treated for 15 hours at various temperatures.

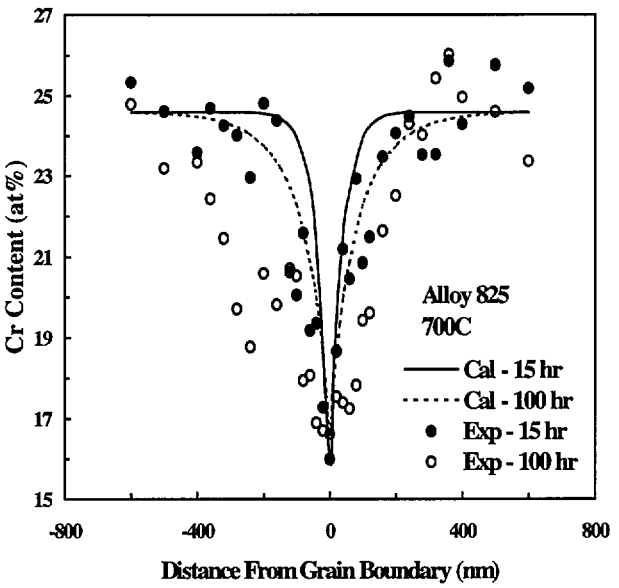

Figure 18. Comparison of measured and calculated chromium concentration profiles for Alloy 825 heat-treated at 700°C for 15 and 100 hours.

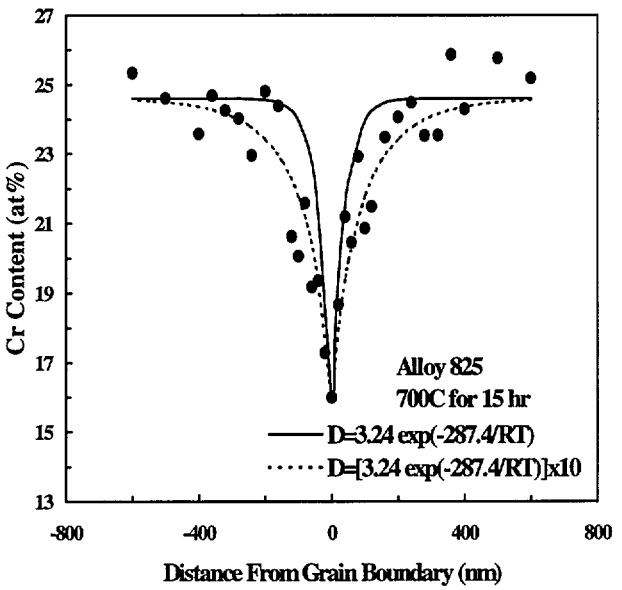

Figure 19. Effect of diffusion coefficient on calculated chromium concentration profiles for Alloy 825 heat-treated at 700°C for 15 hours.

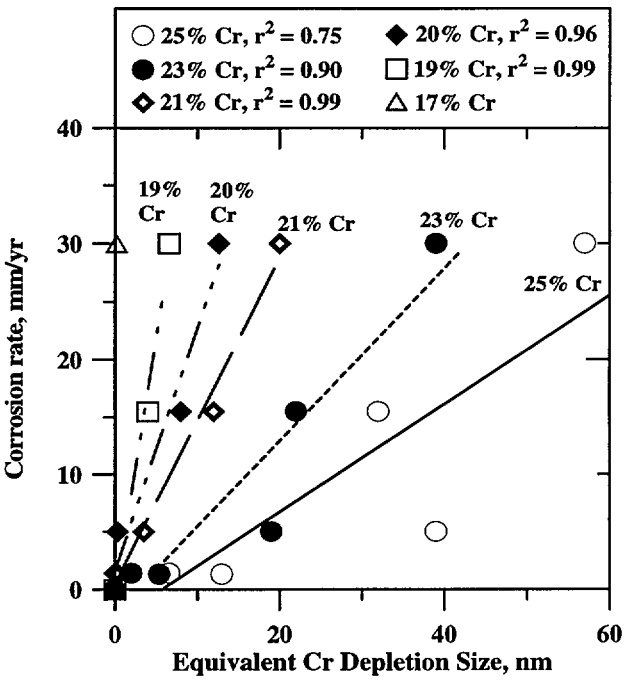

Figure 20. Corrosion rates in boiling 65 % nitric acid as a function of equivalent chromium depletion zone size (nm) below various Cr levels for Alloy 825 after solution annealing followed by various heat treatments.

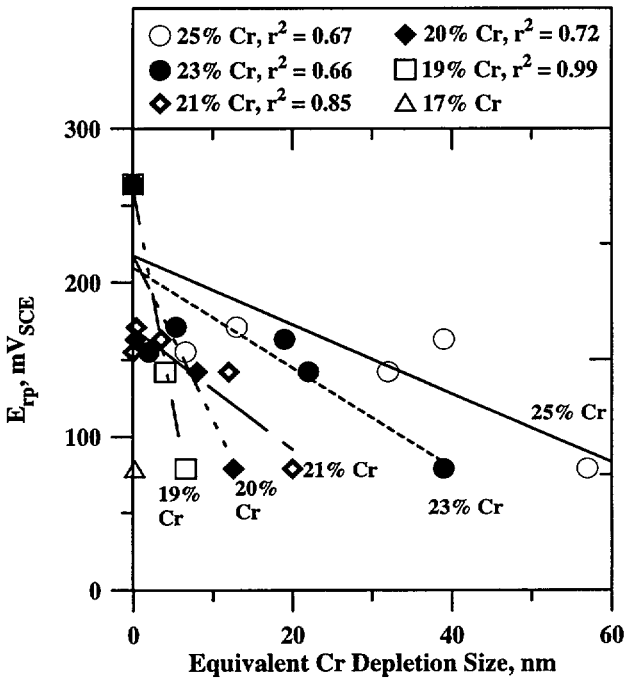

Figure 21. Repassivation potential in a 100 ppm chloride solution at 95°C as a function of equivalent chromium depletion zone size (nm) below various Cr levels for Alloy 825 after solution annealing followed by various heat treatments.

Table I. Bulk Chemical Composition of the Alloy 825 in Weight Percent

Heat	C	Cr	Fe	Mo	Ni	Ti
A	0.01	22.09	30.41	3.21	41.06	0.82
B	0.01	22.07	29.69	3.49	41.22	1.02

Table II. Chemical Composition of Grain Boundary Carbides in Atomic Percent (The ± Sign Indicates the 95 Percent Confidence Interval)

Polishing Solution	Fe	Ni	Cr	Mo
Perchloric Acid	10.1 ± 2.2	9.9 ± 2.5	71.9 ± 4.7	4.7 ±0.9
Nitric Acid	27.2 ± 1.0	36.4 ±1.7	31.0 ± 2.1	2.1 ± 0.3

Table III. The Measured Minimum Grain Boundary Chromium Concentration in Atomic Percent

Temperature (°C)	15 Hours	100 Hours	1,000 Hours
600	—	—	16.5
640	21.1	20.5	17.9
700	16.5	16.6	—
750	19.6	20.0	—
800	20.4	21.7	—

FIGURE CAPTIONS

Figure 1. Effect of heat treatment temperature and time on the corrosion rate of solution-annealed specimens of Alloy 825 (Heat A) in boiling 65 % nitric acid.

Figure 2. Effect of heat treatment temperature and time on the corrosion rate of solution-annealed specimens of Alloy 825 (Heat B) in boiling sulfuric acid plus ferric sulfate.

Figure 3. Time-temperature-sensitization diagram for heat treated mill-annealed and solution-annealed Alloy 825 specimens (Heat A). Corrosion rates determined in boiling 65% nitric acid.

Figure 4. Comparison of the repassivation potential (in solid lines), E_{rp}, measured at a scan rate of 0.167 mV/s, in a 100 ppm chloride solution at 95 °C and the corrosion rate (in dashed lines) in 65 % nitric acid, for specimens of Heat B.

Figure 5. Transmission electron microscopy images of Alloy 825 solution annealed and heat-treated at 640 °C for (a) 15 hours, (b) 100 hours, and (c) 1,000 hours.

Figure 6. Transmission electron microscopy images of Alloy 825 solution annealed and heat-treated at 700 °C for (a) 15 hours and (b) 100 hours.

Figure 7. Transmission electron microscopy images of Alloy 825 solution annealed and heat-treated at 750°C for (a) 15 hours and (b) 100 hours.

Figure 8. Transmission electron microscopy images of Alloy 825 solution annealed and heat-treated at 800 °C for (a) 15 hours and (b) 100 hours.

Figure 9. Chromium concentration profiles along a grain boundary of Alloy 825 containing $M_{23}C_6$ precipitates after heat-treated at 640 °C for various time periods.

Figure 10. Chromium concentration profiles along a grain boundary of Alloy 825 containing $M_{23}C_6$ precipitates after heat-treated at 700 °C for various time periods.

Figure 11. Chromium concentration profiles along a grain boundary of Alloy 825 containing $M_{23}C_6$ precipitates after heat-treated at 750 °C for various time periods.

Figure 12. Chromium concentration profiles along a grain boundary of Alloy 825 containing $M_{23}C_6$ precipitates after heat-treated at 800 °C for various time periods.

Figure 13. Chromium concentration profiles along a grain boundary of Alloy 825 containing $M_{23}C_6$ precipitates after heat-treated for 15 hours at various temperatures.

Figure 14. Chromium concentration profiles along a grain boundary of Alloy 825 containing $M_{23}C_6$ precipitates after heat-treated for 100 hours at various temperatures.

Figure 15. Comparison of measured and calculated chromium depletion widths.

Figure 16. Comparison of measured and calculated chromium minimums.

Figure 17. Calculated chromium concentration profiles for Alloy 825 heat-treated for 15 hours at various temperatures.

Figure 18. Comparison of measured and calculated chromium concentration profiles for Alloy 825 heat-treated at 700°C for 15 and 100 hours.

Figure 19. Effect of diffusion coefficient on calculated chromium concentration profiles for Alloy 825 heat-treated at 700°C for 15 hours.

Figure 20. Corrosion rates in boiling 65 % nitric acid as a function of equivalent chromium depletion zone size (nm) below various Cr levels for Alloy 825 after solution annealing followed by various heat treatments.

Figure 21. Repassivation potential in a 100 ppm chloride solution at 95 °C as a function of equivalent chromium depletion zone size (nm) below various Cr levels for Alloy 825 after solution annealing followed by various heat treatments.